PHILOSOPHICAL TRANSACTIONS A

rsta.royalsocietypublishing.org

Research

Cite this article: Dahiya P, Caggioni M, Spicer PT. 2016 Arrested coalescence of viscoelastic droplets: polydisperse doublets. *Phil. Trans. R. Soc. A* **374**: 20150132.
http://dx.doi.org/10.1098/rsta.2015.0132

Accepted: 29 March 2016

One contribution of 15 to a discussion meeting issue 'Soft interfacial materials: from fundamentals to formulation'.

Subject Areas:
chemical engineering

Keywords:
coalescence, emulsion, droplet

Author for correspondence:
Patrick T. Spicer
e-mail: p.spicer@unsw.edu.au

Arrested coalescence of viscoelastic droplets: polydisperse doublets

Prerna Dahiya[1], Marco Caggioni[2] and Patrick T. Spicer[1]

[1]School of Chemical Engineering, UNSW Australia, Sydney, Australia
[2]Microstructured Fluids Group, Procter and Gamble Co., West Chester, OH, USA

PTS, 0000-0002-8562-3906

Arrested droplet coalescence produces stable anisotropic shapes and is a key mechanism for microstructure development in foods, petroleum and pharmaceutical formulations. Past work has examined the dynamic elastic arrest of coalescing monodisperse droplet doublets and developed a simple model of doublet strain as a function of physical variables. Although the work describes experimental data well, it is limited to describing same-size droplets. A new model incorporating a generalized description of doublet shape is developed to describe polydisperse doublet formation in more realistic emulsion systems. Polydisperse doublets are shown to arrest at lower strains than monodisperse doublets as a result of the smaller contribution of surface area in a given pair. Larger droplet size ratios have lower relative degrees of strain because coalescence is arrested at an earlier stage than in more monodisperse cases. Experimental observations of polydisperse doublet formation indicate that the model under-predicts arrest strains at low solid levels and small droplet sizes. The discrepancy is hypothesized to be the result of nonlinear elastic deformation at high strains.

This article is part of the themed issue 'Soft interfacial materials: from fundamentals to formulation'.

1. Introduction

Emulsions form the basis for common commercial products, such as foods, cosmetics and pharmaceutical formulations, but also find broad use as templates for advanced materials and unique controlled release

THE ROYAL SOCIETY PUBLISHING

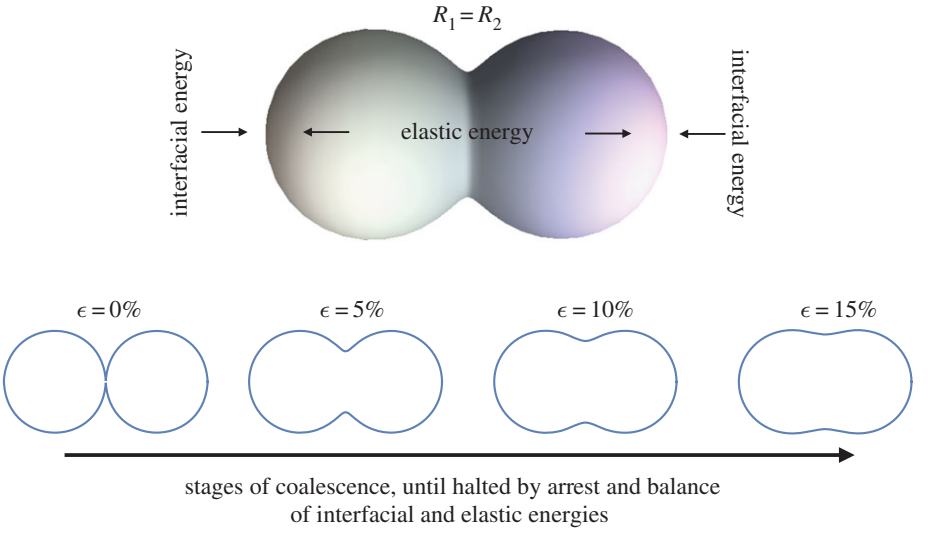

Figure 1. Conceptual model of droplet coalescence arrest, where the driving force bringing droplets together to reduce surface energy is offset by the resistance to deformation of the elastic energy storage capacity of the structure. The predictions of equation (3.1) are also shown for monodisperse droplets at different strain levels consistent with different stages of the coalescence process. (Online version in colour.)

systems. The stability of emulsions can govern the success of a product, and a key phenomenon is coalescence: when two droplets combine to form a single, larger, one.

Coalescence is undesirable when it increases the average droplet size in an emulsion, and can result in phase separation when the process is fast. Depending on the rheological properties of the droplets coalescence can be halted after initiation, but before completion, resulting in arrested, or partial, coalescence structures. In dairy foods, milk lipids are present in both solid and liquid forms, resulting in emulsion droplets containing solid crystals [1,2] that impart a viscoelastic response that is responsible for the observed arrest [3]. Arrest contributes to the formation of three-dimensional networks of droplets in emulsions and is distinct from coagulated or flocculated droplet clusters [4,5] because the droplets are not connected simply by electrostatic or wetting interactions but by a common liquid bridge or neck because of the initiation of coalescence. Very viscous emulsions can coalesce on very long time scales [6,7] but are distinct from the droplets studied here that possess an elasticity able to stably offset the driving force of surface area reduction and halt coalescence at an intermediate state.

Arrested coalescence can be useful or beneficial to food products, for example, stabilizing whipped cream by a fat globule network that suspends small air bubbles. It has also been suggested to play a role in gas cell stabilization of doughs and batters [8,9] and be a possible mechanism for stabilizing thin liquid films and coatings [10]. The robustness of arrested coalescence also allows creation of shaped droplets by assembly of spherical drops [3,11] or by moulding techniques to produce unique structures that change shape due to external triggers [12,13]. The formation of anisotropic droplet shapes is also relevant to the production of solid particles with non-spherical shapes, e.g. 'snowmen', which has been achieved using different wetting, cross-linking and adhesion approaches on polymer melts or emulsions [4,14–19].

When two droplets arrest and form a pair, or doublet, the process can be described by the simple physical model of the opposing phenomena shown in figure 1: interfacial tension-driven reduction of surface energy, and the elastic resistance to droplet deformation by the internal network of solid crystals [3]. If surface energy dominates, the droplets will completely coalesce into a sphere. If elastic energy dominates, the droplets are unable to even initiate coalescence and are stabilized by a sort of three-dimensional Pickering emulsion effect. Arrest occurs, however,

when coalescence can begin but not complete because surface and elastic contributions balance one another at an intermediate state of coalescence. The resulting droplet doublets can vary in shape depending on the state of coalescence when arrest occurs. Pawar *et al.* [3] developed a model of the arrest process using an empirical measure of the decrease in droplet surface area and the linear deformation of the doublet as a function of the dispersed phase bulk rheology.

The model described the driving force of coalescence using an empirical fit of doublet surface area obtained from successive high-speed images of two monodisperse oil droplets at different stages of coalescence [3]. The model predicted the existence of an arrested state that changes with variations in droplet solids concentration, consistent with experimental results, but is only applicable to doublets formed from same-sized, monodisperse, droplets because of the specificity of the fitted area. Emulsions are usually polydisperse and the coalescence of two polydisperse droplets is expected to differ from the behaviour of the monodisperse case given the differences in surface area possible across a typical lognormal distribution of droplets.

We develop a more generalized form of the model of Pawar *et al.* [3] that incorporates a theoretical description of droplet doublet shapes and their surface areas. The model is evaluated and compared to the predictions of the previous model and experimental data on polydisperse doublets with varying size ratios and solids concentrations. The work forms the basis for a broader effort to model the impact of arrested coalescence on bulk emulsion microstructures, enable the design of structured emulsion rheology, create novel colloidal shapes and develop innovative formulations using structured emulsions.

2. Experiment

(a) Emulsion preparation

Equal volumes, 5 ml each, of oil and aqueous phase were mixed. The dispersed oil phase contains hexadecane (99%, Sigma-Aldrich) and wax (Petrolatum, Unilever) in a ratio set by the desired solids concentration. The aqueous continuous phase consists of 0.5 wt% microfibrous cellulose (CP Kelco) and 10 mM sodium dodecylsulfate (99%, Fluka) surfactant solution [3]. The emulsion is prepared by combining dispersed and continuous phase, then heating to 75°C and shaking for 10 s by hand. The resulting emulsion is polydisperse and stable against sedimentation as a result of the yield stress of the continuous phase. Initially, the dispersed phase is homogeneous but, as the temperature goes down, the wax (m.p. ∼ 45–60°C) inside the droplets forms irregular flat solid crystals in the hexadecane. Emulsions with different solids content (15–45%) are prepared to form various partially crystalline droplets. In all cases studied, the equilibrium state of the droplets is one in which the liquid fraction completely wets the crystals inside. The resulting droplets are viscoelastic in their bulk rheology [3,13] and possess a continuous fluid surface with no particles adsorbed at the liquid–liquid interface.

(b) Microscopy

Doublets were formed and studied using micromanipulation stages and microcapillaries to grasp and move droplets into contact to initiate coalescence [3,11]. Borosilicate glass capillaries (1 mm outer diameter and 0.5 mm inner diameter, Sutter Instruments) are pulled with a Micropipette Puller (Model P-97, Sutter Instruments) to form microcapillaries with tip size smaller than the droplets manipulated by a factor of at least two. The other end of the capillary is attached to a syringe containing water using transparent tubing (Tygon). Adjusting the height of the water reservoir varies the hydrostatic pressure to enable grasping and manipulation of a droplet. The capillary is connected to a 3-axis coarse manipulator (Narishige International) mounted on a microscope to enable direct study of the coalescence and arrest process. A 1 ml sample of emulsion is placed on a glass slide and the capillary tip aligned to the droplet height. By applying negative hydrostatic pressure with the water reservoir, the droplet is drawn towards the capillary tip and grabbed without deformation. The droplet is then brought through the continuous phase

to contact a second droplet and initiate coalescence. Observation of contacted droplets continues for at least 15 min to map the stages of coalescence and any arrest [3]. Imaging is performed using a Motic AE31 inverted optical microscope with custom-mounted micromanipulator attachments. Digital images are obtained using a Moticam 10 MP camera and image analysis carried out using ImageJ software [20].

3. Theory

The shape history of polydisperse doublets can be approximated using the below 'empirical analytical function' that has been validated by comparisons with finite-element simulations of droplet neck growth during coalescence [21]. The model can map the outline of two droplets at most stages of coalescence [21,22], as shown by the four calculated curves in figure 1:

$$r(\theta) = \sqrt{4bc}\sqrt{1 - b\sin^2(\theta)} + k\cos(\theta), \tag{3.1}$$

where

$$k = \frac{N-1}{N+1}(2 - b^{1/N})^N, \tag{3.2}$$

$$c(b) = \frac{3b}{1+N^3}\left[\sqrt{b}\left(\frac{5}{3} - b\right) + \frac{k^2}{\sqrt{b}}(1+b) + \frac{(1-b)^2(b-k^2)}{4b}\ln\left(\frac{1+b+2\sqrt{b}}{1+b-2\sqrt{b}}\right)\right]^{-2/3} \tag{3.3}$$

and

$$N = \frac{R_1}{R_2}, \tag{3.4}$$

and b is a parameter that indicates the degree of coalescence, varying from a value of 1 for no coalescence to 0 for completeness [21]. We do not carry out calculations over the entire range of b values, instead starting at $b \sim 0.9$ and ending at $b \sim 0.2$ to avoid small unrealistic changes in the doublet shape at extreme b values. Here, the convention used is that R_1 is always the larger droplet radius when a polydisperse doublet is studied. We perform our calculations for a unit reference sphere and scale the dimensions accordingly for area and energetic determinations. The maximum strain of polydisperse doublets, that is, the amount attained after complete coalescence, is found by geometry and volume conservation to be

$$\epsilon_{\max} = 1 - \frac{\sqrt[3]{1+N^3}}{1+N}, \tag{3.5}$$

which is easily shown to reproduce the result of Pawar *et al.* [3] for the monodisperse case when $N = 1$:

$$\epsilon_{\max} = 1 - 2^{-2/3}. \tag{3.6}$$

A surface integral of equation (3.1) can also be used to calculate a doublet surface area at each stage of coalescence to compare relative driving forces for different doublet proportions. A simple description of the total energy, E_{tot}, of a coalescing pair of spherical droplets accounts for the reduction in surface area driven by interfacial tension and the resistance to compression by the elastic microstructure of the droplets is [3]

$$E_{\mathrm{tot}} = \gamma A(\epsilon) + \tfrac{3}{2}G'\epsilon^2 V, \tag{3.7}$$

where γ is the liquid–liquid interfacial tension of $10\,\mathrm{mN\,m^{-1}}$ [3], A is the total doublet surface area, G' is the elastic modulus of the droplet phase, V is the total droplet volume and ϵ is the linear strain of the doublet, defined by

$$\epsilon = \frac{L_0 - L}{L_0}, \tag{3.8}$$

where L is the instantaneous/final doublet length and L_0 is the initial doublet length. We assume here that the two droplets behave as ideal isotropic elastic springs so that, even for polydisperse doublets, the overall length of the doublet is the only significant contribution to strain. As in [3],

we link the droplet solids content to its elasticity using a power-law fit to the experimental bulk rheology data of [3]:

$$G' = 2.8 \times 10^5 \phi^{4.8}. \tag{3.9}$$

All calculations are carried out using MATHEMATICA software v. 10.0.

4. Results and discussion

At any moment during coalescence, the surface area of the droplets is an indicator of how far away the system is from its final state of total coalescence. Accurate representation of the surface area thus enables calculation of the process driving force. In addition, because arrest halts the progress of coalescence at an intermediate state, predicting droplet area also predicts the arrested shape produced when viscoelastic droplets are used. Figure 2 shows the evolution of doublet area as it is reduced by the process of coalescence for the experimental fit of [3] and compares it with the calculation of equations (3.1)–(3.4). Overall the same exponential decay in area with strain is seen for experiment and theory, indicating the rapid relaxation of a doublet into a spherical droplet. Both results end at the maximum strain for monodisperse droplets, $\epsilon = 0.37$. The experimental fit from [3] in figure 2 under-predicts the theoretical area reduction for most strain values, possibly because the continuous phase fluid used in [3] has a small yield stress that can affect the relaxation of the droplets. The area change predicted in figure 2 can now be used to calculate the change in energy as coalescence proceeds and then determine the point of minimum energy in order to assess the completion, arrest or prevention of coalescence.

Using equations (3.1)–(3.4) to determine the doublet surface area and the elasticity data from [3], and substituting these into equation (3.7) as a function of strain, the curves in figure 3 are obtained. The calculations in figure 3 are performed assuming monodisperse droplets with radius $R = 50\,\mu\text{m}$, an interfacial tension, $\gamma = 10\,\text{mN}\,\text{m}^{-1}$, and a droplet solids volume fraction, $\phi = 0.4$. The doublet area decays exponentially as coalescence proceeds from high to low strains, while the elasticity increases by a power law with exponent 4.8 [3]. Because of the opposing natures of the two functions, a minimum in the total energy curve exists, representing the intermediate arrested state. If either surface or elastic energy dominate the coalescence process, the drops will either fully coalesce or not coalesce at all, respectively. Pawar *et al.* [3] used the model to predict the limits of arrest, as a function of droplet solids level and interfacial tension, but worked with only a single size of droplets and did not explore the effects of varying droplet size on arrest.

Examples of arrested doublet structures are shown in figure 4 for several different individual initial droplet sizes and their resulting strains. In figure 4, the same solids content, $\phi = 0.4$, is used in each doublet but the interfacial area varies with the droplet radii. At large radii, the strain approaches zero, the onset of no coalescence, while at low radius it approaches the maximum strain of $\epsilon_{\text{max}} = 0.37$ achieved during total coalescence. Such a result is consistent with our intuition regarding the effects of interfacial curvature on interfacial, or Laplace, pressure. More highly curved, smaller droplets exhibit a higher strain than larger droplets because the higher interfacial pressure squeezes the two drops more closely together. A prediction of the model is also plotted in figure 4 and follows the same inverse dependency on droplet radius but over-predicts the droplet strain. The larger strain found from the model could result from differences between the experimental system and our description of droplet elasticity. All elasticity measurements were made using bulk volumes of the droplet phase, but the droplets are much closer to the size of the internal crystal network building blocks. If the droplet elasticity value, or its elastic response, differs significantly at smaller length scales from the bulk value, a difference in strain would be observed. It is clear from the equilibrated microscopy images of representative doublets in figure 4 that the internal structure is not destroyed by the compression, as the droplets never fully coalesce. Given the strong influence of droplet size on arrest in these emulsions, and the likelihood that practical emulsions will contain relatively broad distributions of droplet sizes, it is of interest to more broadly explore how changing droplet size can affect arrest.

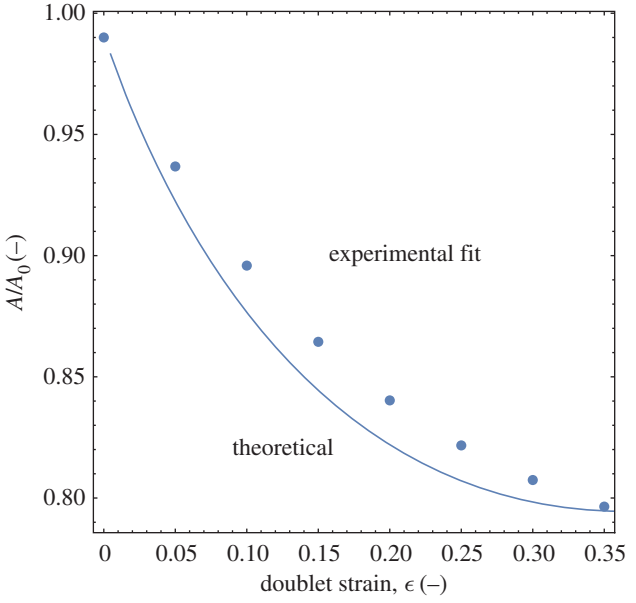

Figure 2. Comparison of analytical and empirical fit results for monodisperse droplet area change during coalescence. (Online version in colour.)

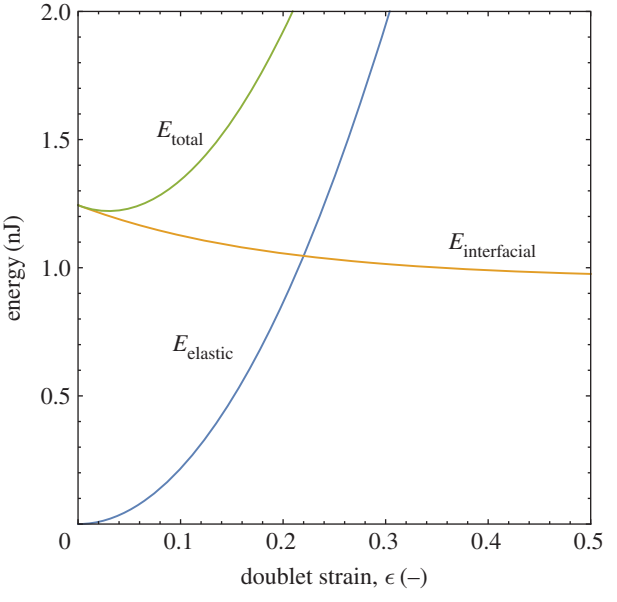

Figure 3. The total energy of the doublet is the sum of its interfacial and elastic contributions. The minimum in the total energy curve determines the doublet's ultimate stable arrested state. (Online version in colour.)

The generality of the description of doublet shapes in equations (3.1)–(3.4) [21] enables us to predict their shape during coalescence, as demonstrated in figure 5. Figure 5 shows a rendering calculated for a doublet with one droplet 60% the radius of the larger one and several shape profiles for different values of the total doublet strain. For polydisperse droplets, we assume only linear strain is significant and so define strain as we did for the monodisperse case, using equation

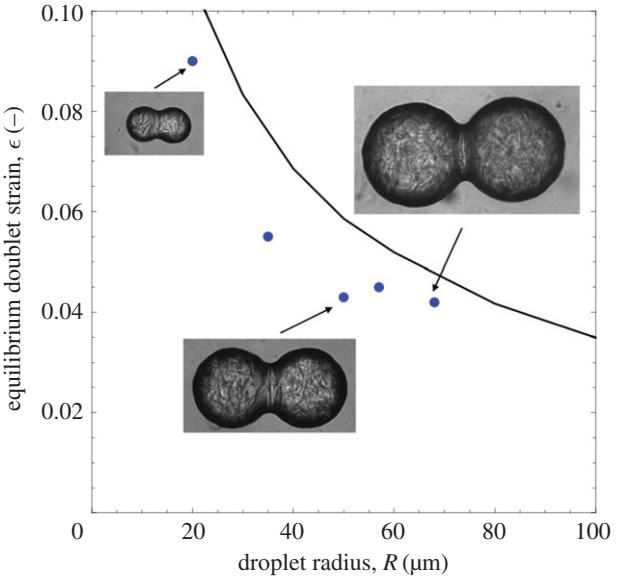

Figure 4. Arrested doublets have larger strains at smaller droplet radii as a result of the increased interfacial curvature and Laplace pressure that drives the droplets together. Higher pressures further compress the internal elastic structure, resisting complete coalescence. The line is a plot of the prediction of the physical model showing the strong effect of drop radius on the ultimate doublet arrested strain. (Online version in colour.)

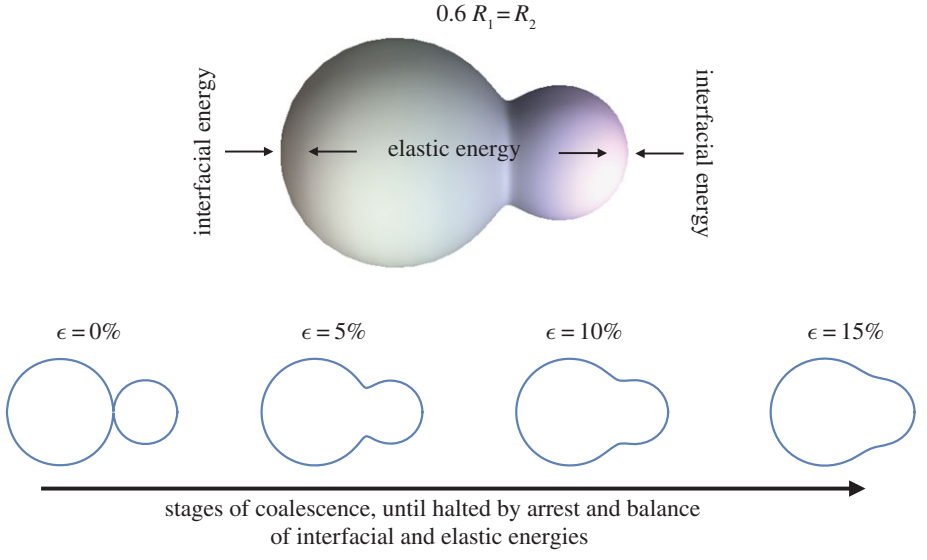

Figure 5. Coalescence of two different-sized droplets. The analytical model [21] describes the shapes of polydisperse doublets at all stages of coalescence. (Online version in colour.)

(3.8). Any change in length of the doublet is thus normalized to the starting length in order to avoid biasing the calculations by the change in radius of one of the droplets. As for monodisperse doublets, a 'neck' is formed between the two droplets once coalescence initiates and the smallest drop determines the size of the neck. Polydisperse doublets will have a smaller total surface area as the size ratio increases and the dynamics of area loss will be different as well. As before, we

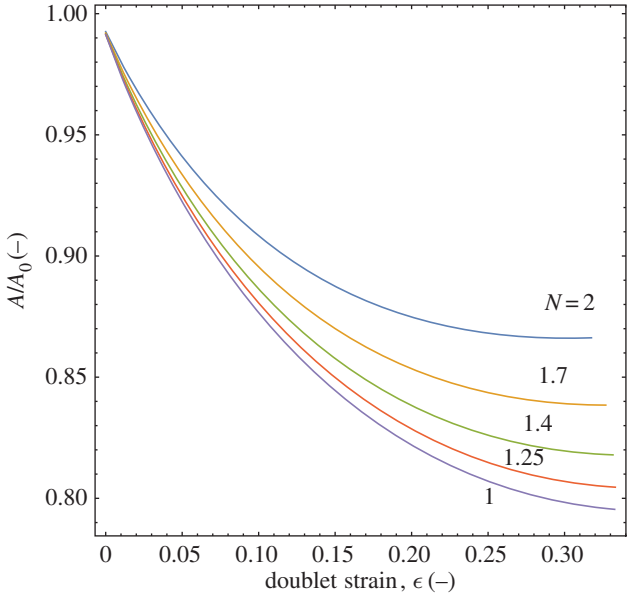

Figure 6. Decay of area, normalized by its initial value, for doublets with increasing radius ratio, N, as their strain increases and coalescence is approached. Higher polydispersity within a doublet reduces the amount that area can decrease during the coalescence process. (Online version in colour.)

use the model to calculate doublet surface area, as a function of the stage of coalescence, and use that as input to equation (3.7) in order to understand the competing effects of surface and elastic energy on the process.

Figure 6 shows the calculated relative decay of different doublets for a range of radius ratio values. As expected, increasing the radius ratio decreases the final maximum reduction in area of a doublet at the point of complete coalescence, from the monodisperse case of 79% of the initial area to nearly 87% for a value of $N = 2$. Similarly, the reduction in area is higher at a given strain for higher N values. A lower reduction in area with increasing radius ratio translates into a smaller driving force for coalescence and, potentially, a lower arrest strain for the polydisperse cases.

Calculating the arrest strain of polydisperse doublets as a function of radius ratio and solids concentration for a given larger droplet radius, R_1, the overall map in figure 7 is obtained. As suggested above, increasing the radius ratio decreases the arrest strain by bringing the doublet closer to its final state by starting from a lower initial area. The model also predicts a lowering of stable arrest strain with increasing solids level. The higher elasticity at higher solids loadings causes a stronger resistance to the surface energy-driven coalescence, leading to arrest at an earlier stage of coalescence and a similarly lower strain. For $\phi = 0.35{-}0.4$, the arrest strain changes very little for values of $N \sim 1{-}3$, indicating strong resistance and a low driving force (figure 7). Also plotted in figure 7 is the maximum strain for polydisperse doublets, equation (3.5), in order to check the model predictions but also to bound the observed behaviour. The general shapes of the curves are the same, with a sigmoidal decay in arrest strain seen as a function of radius ratio. As solids concentration is decreased, the curves more closely approach the limiting value of equation (3.5) as it is equivalent to a coalescence process for droplets containing no solids and possessing no elasticity. The model agrees quite well with the geometric prediction when it is run using a zero elasticity. Increasing the overall doublet size, by repeating the above calculations using a reference droplet size of $R_1 = 300\,\mu\text{m}$, produces a similar set of curves in figure 8 but with distinctly lower strain values. The larger droplets have a greater volume contribution to the arrest strain, increasing resistance to deformation and reducing its relative driving force. Figure 8 shows an approximately 10% lower strain is predicted for $R_1 = 300$ versus $50\,\mu\text{m}$ at a solids level of 15%.

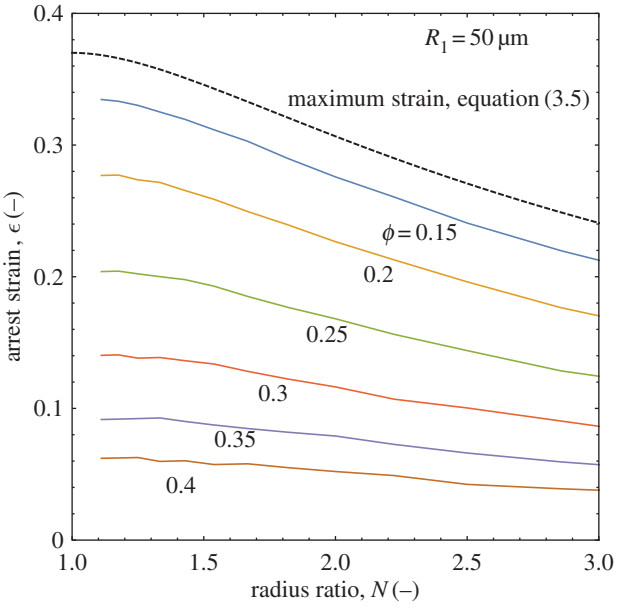

Figure 7. Changes in doublet polydispersity and solids level alter the resulting doublet arrest strain by changing the amount of area reduction that can occur and the droplet elasticity, respectively. (Online version in colour.)

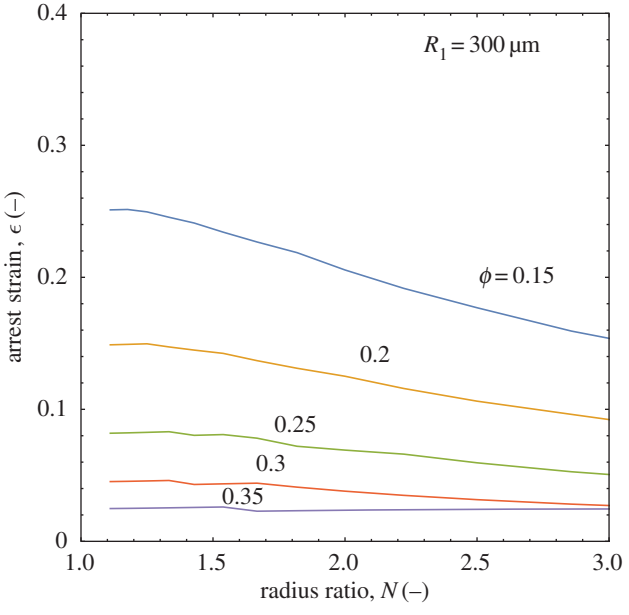

Figure 8. Increasing the overall doublet size decreases the strain of the structure for all solids levels. (Online version in colour.)

There is also almost constant strain predicted at high solids levels, with little change for $\phi = 0.35$ and the $\phi = 0.4$ line not shown as it is flat and overlaps most of the $\phi = 0.35$ line. It is also of interest to observe the experimental formation of polydisperse doublets to verify that their arrest is as stable as the monodisperse case and is affected by similar physical constraints.

A summary matrix of micrographs of polydisperse doublets with varying solids loading and radius ratio is shown in figure 9. The images show equilibrated arrested doublets for a wide

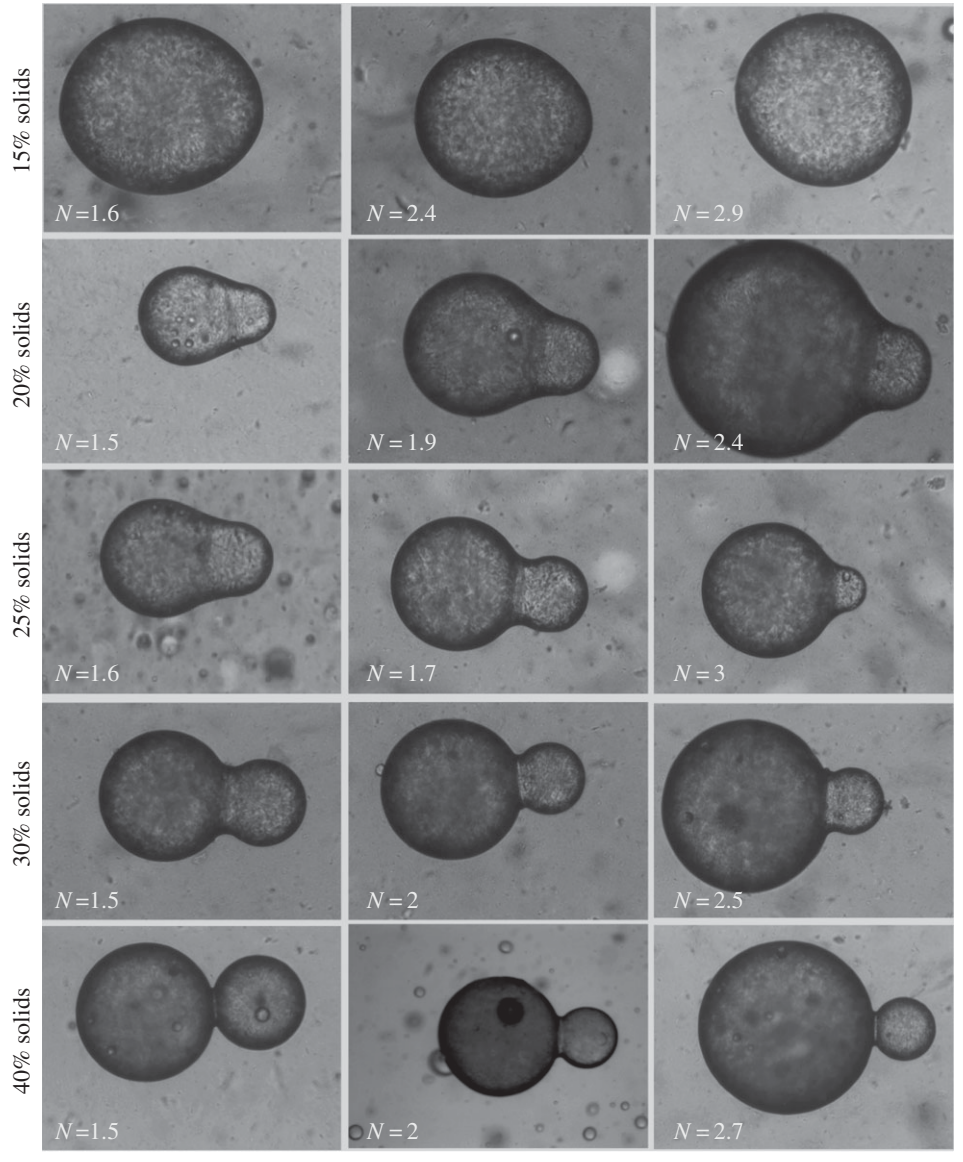

Figure 9. Examples of polydisperse doublets arrested by different solids levels for different values of the radius ratio, *N*. The height of each individual image is 250 μm.

range of solids levels and dimensions, all of which form stable, axisymmeteric shapes that are not significantly distorted by the arrest process. The broad range of shapes possible is evident, indicating not only the potential for simple synthesis of anistotropic colloids by such a process, but also the fact that such structures will form a rich array of connections within more complex emulsion microstructures. The shapes of the doublets show smooth, continuous borders that indicate the fluid-like behaviour of the droplet surfaces. Although almost solid-like in their static appearance because of the stabilization of shape by internal elasticity, the structures retain their fluid interface. Similar to monodisperse systems, higher solids levels decrease the doublet arrest strain because of an increased elastic resistance to coalescence and its associated compression. Even at the lowest solids concentration of 15%, the lack of perfect spherical shapes is indicative of the fact that the internal elastic network of the droplet is arresting full coalescence. Also seen in most cases is the smaller strain predicted at higher radius ratios. Validation of the above

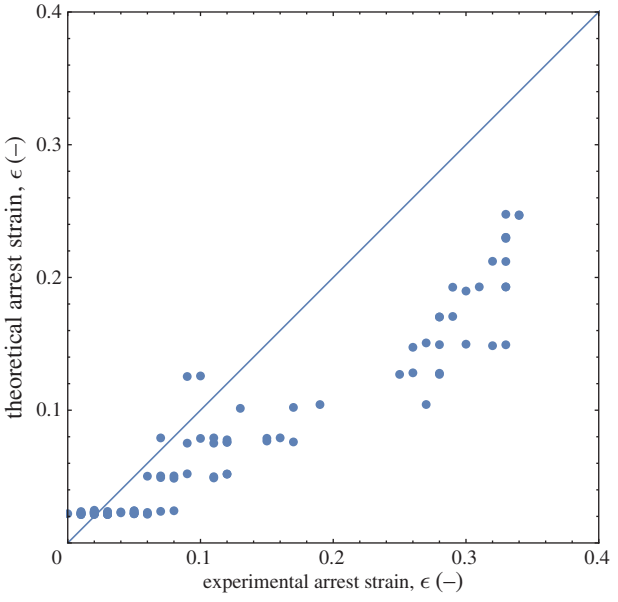

Figure 10. A comparison of the predicted level of strain and the experimentally observed value shows reasonable agreement at low strains but poorer agreement at high strains. The droplets may deform following more nonlinear elastic dynamics at high strains, causing disagreement with the simple model used here. (Online version in colour.)

predictions is necessary to evaluate the accuracy of the model and the significance of the predicted effects on shape and structural arrangement.

Because a wide range of droplet sizes and properties is examined, an aggregate comparison is made of the strains predicted by the model and observed experimentally. Figure 10 compares the experimental and theoretical values for droplets with radii between $R_1 = 100$ and $500\,\mu\mathrm{m}$ and solids levels between $\phi = 0.15$ and 0.45. Although variations in drop size and solids level will cause variations in strain, we see the model predictions are in reasonable agreement with experiment at low strains, meaning the larger droplets and higher solids levels. In such cases, the small deformation is more consistent with the assumed linear elastic behaviour. Still, the data are broadly distributed around the theory line and we note that the emulsion droplets we produce are polydisperse not only in size, but also in their crystallization history because differently sized droplets cool at different rates to form their inner crystalline networks. The resulting changes in crystal orientation and packing can cause variations in mechanical response and the experimental variability we see at low strains. The variability observed may also be the result of larger errors in image analysis measurement of small strains. Above strains of 20%, the model under-predicts the strain observed experimentally. If the droplets exhibit nonlinear elastic deformation, its effects are more likely to be significant at the large deformations seen at lower solids levels and smaller droplet sizes.

Differences between the observed doublet shapes and the model are likely the result of a more complex rheological response of the viscoelastic droplets than the bulk rheological response of the droplet phase. More work is needed to ascertain whether the droplets exhibit a small degree of nonlinear elastic response, which could cause the observed discrepancy.

One mechanism of non-ideal elastic response is structural rearrangement during deformation. A preliminary evaluation of whether such structural changes occur suggests a way to evaluate individual droplet response, as it is expected to differ from the bulk fluid behaviour. Our model approximates the doublet's elastic response to deformation experienced during coalescence and arrest as linear, but we can explore this response in more detail by examining the deformation's reversibility and dynamic nature. The presence of surfactant around the doublets lowers their interfacial tension to $\gamma \sim 10\,\mathrm{mN\,m^{-1}}$, so localized dilution with deionized water will raise the

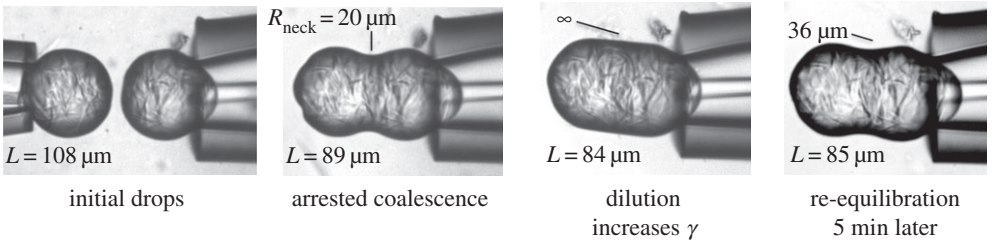

Figure 11. Microscopy images of a doublet changing its strain, and thus shape, in response to a dilution-induced increase in the local interfacial tension. As surfactant diffuses back in to re-equilibrate the local concentration, the strain increases but the droplet does not return to its original strain, probably because of structural rearrangements that cause hysteresis in the droplet's rheological response.

interfacial tension by a factor of at least two. Figure 11 shows the initial formation of an arrested doublet from two individual droplets. The resulting doublet is then held in place and flushed with deionized water to temporarily dilute the surrounding and adsorbed surfactant. The response is immediate: the deformation increases by 5–6% as the local interfacial tension increases the Laplace pressure. Several minutes after flushing, the interfacial tension has decreased again to its original value and the doublet has equilibrated at a new deformation slightly less than during rinsing but significantly more than prior to dilution. It is likely that some restructuring took place within the doublet, or the step change in stress caused an irreversible deformation, whereas more reversible behaviour might be expected for less brittle structures like hydrogels. Figure 11 demonstrates the responsiveness, at small deformations, of viscoelastic structures to subtle changes like dilution but also suggests an approach for triggering an irreversible shape and structural change at larger deformations [12,13]. It also suggests the need for more detailed study of individual droplet response to deformations experienced at different strain levels.

5. Conclusion

The coalescence, and arrested coalescence, of polydisperse viscoelastic droplets has been studied and the resulting structures compared to an energetic model based on the relative importance of droplet elastic energy and surface energy as coalescence proceeds. The model predictions are consistent with experimental observations of the stable arrest of polydisperse doublets over a wide range of solids concentrations and radius ratios. Doublet shape is a strong function of the droplet polydispersity, with final arrest strains decreasing significantly as the smaller droplet of the pair decreases in size. Variations in droplet polydispersity are typical for most emulsions and, if microstructure formed by significant arrested coalescence is present, the structural integrity and material rheology are likely to be strongly affected by the efficiency of connected droplet packing and the resultant load-bearing response [23–25]. Future work will study the individual droplet deformation response in more detail, explore polydisperse droplet arrest in more complex droplet aggregates, and improve understanding of how such structures contribute to emulsion rheology and flow.

Data accessibility. Figure data for this publication are published to Research Data Australia, an online data discovery and archival service.

Authors' contributions. P.D. carried out the experiments and P.S. carried out the calculations. P.D., M.C. and P.S. performed the data analysis. P.S. conceived of and designed the study, and drafted the manuscript with M.C. and P.D.

Competing interests. We declare we have no competing interests.

Funding. This work was partially supported by start-up funds received from UNSW Australia School of Chemical Engineering and ARC Discovery grant no. DP150100865.

Acknowledgements. We gratefully acknowledge Prof. Timothy Atherton (Tufts University) for explaining the geometry of coalescing doublets to us.

References

1. Boode K, Walstra P. 1993 Partial coalescence in oil-in-water emulsions 1. Nature of the aggregation. *Colloids Surf. A* **81**, 121–137. (doi:10.1016/0927-7757(93)80239-B)
2. Fredrick E, Walstra P, Dewettinck K. 2010 Factors governing partial coalescence in oil-in-water emulsions. *Adv. Colloid Interface Sci.* **153**, 30–42. (doi:10.1016/j.cis.2009.10.003)
3. Pawar AB, Caggioni M, Hartel RW, Spicer PT. 2012 Arrested coalescence of viscoelastic droplets with internal microstructure. *Faraday Disc.* **158**, 341–350. (doi:10.1039/c2fd20029e)
4. Torza S, Mason S. 1969 Coalescence of two immiscible liquid drops. *Science* **163**, 813–814. (doi:10.1126/science.163.3869.813)
5. Princen HM. 1984 Geometry of clusters of strongly coagulated fluid drops and the occurrence of collapsed plateau borders. *Colloids Surf.* **9**, 47–66. (doi:10.1016/0166-6622(84)80141-9)
6. Philip J, Bonakdar L, Poulin P, Bibette J, Leal-Calderon F. 2000 Viscous sintering phenomena in liquid–liquid dispersions. *Phys. Rev. Lett.* **84**, 2018–2021. (doi:10.1103/PhysRevLett.84.2018)
7. Philip J, Poirier JE, Bibette J, Leal-Calderon F. 2001 Gelation and coarsening in dispersions of highly viscous droplets. *Langmuir* **17**, 3545–3552. (doi:10.1021/la0013771)
8. Brooker B. 1993 The stabilisation of air in cake battersthe role of fat. *Food Struct.* **12**, 285–296.
9. Brooker B. 1996 The role of fat in the stabilisation of gas cells in bread dough. *J. Cereal Sci.* **24**, 187–198. (doi:10.1006/jcrs.1996.0052)
10. van der Kooij HM, Sprakel J. 2015 Watching paint dry; more exciting than it seems. *Soft Matter* **11**, 6353–6359. (doi:10.1039/C5SM01505G)
11. Pawar AB, Caggioni M, Ergun R, Hartel RW, Spicer PT. 2011 Arrested coalescence in Pickering emulsions. *Soft Matter* **7**, 7710–7716. (doi:10.1039/c1sm05457k)
12. Caggioni M, Bayles AV, Lenis J, Furst EM, Spicer PT. 2014 Interfacial stability and shape change of anisotropic endoskeleton droplets. *Soft Matter* **10**, 7647–7652. (doi:10.1039/C4SM01482K)
13. Caggioni M, Lenis J, Bayles AV, Furst EM, Spicer PT. 2015 Temperature-induced collapse, and arrested collapse, of anisotropic endoskeleton droplets. *Langmuir* **31**, 8558–8565. (doi:10.1021/acs.langmuir.5b00321)
14. Jung M, Hubert D, Veldhoven E, Frederik P, Herk A, German A. 2000 Vesicle–polymer hybrid architectures: a full account of the parachute architecture. *Langmuir* **16**, 3165–3174. (doi:10.1021/la991233a)
15. Pawar AB, Kretzschmar I. 2010 Fabrication, assembly, and application of patchy particles. *Macromol. Rapid Commun.* **31**, 150–168. (doi:10.1002/marc.200900614)
16. Park J, Forster J, Dufresne E. 2010 High-yield synthesis of monodisperse dumbbell-shaped polymer nanoparticles. *J. Am. Chem. Soc.* **132**, 5960–5961. (doi:10.1021/ja101760q)
17. Sacanna S. 2011 Shape-anisotropic colloids: building blocks for complex assemblies. *Curr. Opin. Colloid Interface Sci.* **16**, 96–105. (doi:10.1016/j.cocis.2011.01.003)
18. Walther A, Müller AHE. 2013 Janus particles: synthesis, self-assembly, physical properties, and applications. *Chem. Rev.* **113**, 5194–5261. (doi:10.1021/cr300089t)
19. Zhang X, Yao X, Wang X, Feng L, Qu J, Liu P. 2014 Robust hybrid raspberry-like hollow particles with complex structures: a facile method of swelling polymerization towards composite spheres. *Soft Matter* **10**, 873–881. (doi:10.1039/C3SM52739E)
20. Schneider CA, Rasband WS, Eliceiri KW. 2012 NIH Image to ImageJ: 25 years of image analysis. *Nat. Methods* **9**, 671–675. (doi:10.1038/nmeth.2089)
21. Yadha V, Helble JJ. 2003 Modeling the coalescence of heterogenous amorphous particles. *J. Aerosol Sci.* **35**, 665–681. (doi:10.1016/j.jaerosci.2003.11.009)
22. Mbanga BL, Voorhes KK, Atherton TJ. 2014 Simulating defect textures on relaxing nematic shells. *Phys. Rev. E* **89**, 052504. (doi:10.1103/PhysRevE.89.052504)
23. Thivilliers F, Backov R, Schmitt V, Leal-Calderon F. 2007 Gelling of oil-in-water emulsions comprising crystallized droplets. *Langmuir* **23**, 4792–4799. (doi:10.1021/la070071c)
24. Thivilliers F, Laurichesse E, Leal-Calderon F, Schmitt V. 2008 Thermally induced gelling of oil-in-water emulsions comprising partially crystallized droplets: the impact of interfacial crystals. *Langmuir* **24**, 13 364–13 375. (doi:10.1021/la802521f)
25. Thivilliers-Arvis F, Laurichesse E, Schmitt V, Leal-Calderon F. 2010 Shear-induced instabilities in oil-in-water emulsions comprising partially crystallized droplets. *Langmuir* **26**, 16 782–16 790. (doi:10.1021/la1027288)